Electronic Supplementary Information (ESI)

Tuning electrochemical and catalytic ORR performance of C_{60} by its encapsulation in ZIF-8: a solid-state analogue of dilute fullerene solution

Olivia Basu, [a] Subhabrata Mukhopadhyay, [a] Avik De, [b] Anupam Das [a] and Samar K. Das*[a]

[a] School of Chemistry, University of Hyderabad, Hyderabad – 500046, India

[b] School of Chemical Sciences, Indian Association for the Cultivation of Science, Jadavpur, Kolkata 700 032, India

*E-mail: skdas@uohyd.ac.in

Table of Contents:

Section S1. Materials and methods

All the chemicals were used as received without any further purification. Zinc nitrate hexahydrate {$Zn(NO_3)_2.6H_2O$} was purchased from Finar chemicals. 2-methylimidazole (2-mIm) and fullerene C_{60} (99.5% purity) were purchased from Sigma Aldrich. Polyvinyl alcohol (PVA) was obtained from Merck. Methanol, acetonitrile and toluene were purchased from Finar chemicals.

Synthesis of ZIF-8: 0.450 g (2.5 mmol) of $Zn(NO_3)_2.6H_2O$ was dissolved in 12 mL of methanol and in a separate round bottom flask (100 mL), 1 g (12.2 mmol) of 2-methyl imidazole (2-mIm) was dissolved with 12 mL of methanol. The methanolic solution of $Zn(NO_3)_2$ was slowly added into the flask, under stirring. The reaction mixture was left undisturbed for 12 hours and the product ZIF-8 was obtained as a white precipitate. It was collected by centrifugation and was washed repeatedly with methanol (6 times over a course of 2 days) and dried in a hot air oven at 70 ℃ for 24 hours.

Synthesis of C_{60}Z-n (n = A, B, C, D and E): C_{60} loading variations

The precursor solutions were prepared by mixing the reagents in the specified proportion listed in table S1. The methanolic solution of 2-methyl imidazole (2-mIm) was taken in a round bottom flask (100 mL) and kept under stirring. Initially, one-fourth of the $Zn(NO_3)_2.6H_2O$ solution was added dropwise into the methanolic solution of 2-methyl imidazole until turbidity appeared. Then, both the fullerene C_{60} solution and the $Zn(NO_3)_2$ solution were added dropwise simultaneously into the flask, under vigorous stirring. The reaction mixture was left undisturbed for 12 hours and the product **C_{60}Z-n** (n = A, B, C, D and E) was obtained as precipitate. The product was collected by centrifugation and was washed repeatedly with methanol (6 times over a course of 2 days). Following this, the product was kept under stirring in toluene for 1 day, during which the solvent was changed thrice (or till a colourless supernatant was achieved), to get rid of any surface adsorbed fullerene. Then, the product **C_{60}Z-n** (n = A, B, C, D and E) was collected and washed twice with methanol, to remove toluene from the pores of the composite. The product was obtained as a light purple coloured powder, after being dried at 70 ℃ for 24 hours.

Table S1.

Name of Sample	C_{60} (mg) in toluene (mL)	$ZnNO_3.6H_2O$ (g) in methanol (mL)	2-mIm (g) in methanol (mL)
C_{60}Z-A	2mg/ 4ml	0.450 g/ 10mL	1g/ 10mL
C_{60}Z-B	5 mg/ 5ml	0.450 g/ 10mL	1g/ 10mL
C_{60}Z-C or **C_{60}Z**	10 mg/ 10ml	0.450 g/ 10mL	1g/ 10mL
C_{60}Z-D	15 mg/ 15ml	0.450 g/ 10mL	1g/ 10mL
C_{60}Z-E	20 mg/ 20ml	0.450 g/ 10mL	1g/ 10mL

0.450 g $ZnNO_3.6H_2O$ - 2.5 mmol; 1 g 2-mIm - 12.2 mmol; 10 mg C_{60} - 0.014 mmol.

The loading of C_{60} in these composites (**C_{60}Z-A**, **C_{60}Z-B**, **C_{60}Z-C**, **C_{60}Z-D** and **C_{60}Z-E)** was calculated by elemental analysis (section S3.2, supporting information). Increasing the amount of C_{60} precursor resulted into increase of C_{60} loading in **C_{60}Z-A**, **C_{60}Z-B** and **C_{60}Z-C**, respectively. Further increase in the amount of C_{60} precursor resulted into marginal increase in C_{60} loading in case of the **C_{60}Z-D** and **C_{60}Z-E**. Since optimal loading of C_{60} could be obtained for **C_{60}Z-C**, for the majority of the article, **C_{60}Z-C** composite has been discussed in detail and for generalization, has been referred to as **C_{60}Z**.

Preparation of PVA membrane: A 1 wt% homogeneous solution of commercially available PVA was prepared in milli-Q water and poured onto a glass Petri dish. The solvent was evaporated slowly at 70 °C. The formed membrane was then peeled out and dried in vacuum at 100 °C to remove the trace of solvent molecules.

Fabrication of C_{60}Z into C_{60}Z-PVA composite membrane: This homogenous nanocomposite membrane was prepared by solution casting method.[1] 20 mg of the **C_{60}Z** composite was dispersed in 10 mL of milli-Q water by sonicating it for 30 minutes. Another solution of 200 mg of PVA in 10 mL of milli-Q water was prepared separately. These two separately prepared mixtures were then added together such that the final PVA concentration in solution was 1 wt% and the amount of **C_{60}Z** was 10 wt% (with respect to polymer weight). This polymer-nanocomposite blend was stirred vigorously at room temperature for 24 h to obtain a uniform dispersion. It was then poured onto a glass Petri dish and the solvent was evaporated slowly at 70 °C. The formed membrane was then peeled out and dried in vacuum at 100 °C to remove the trace of solvent molecules.

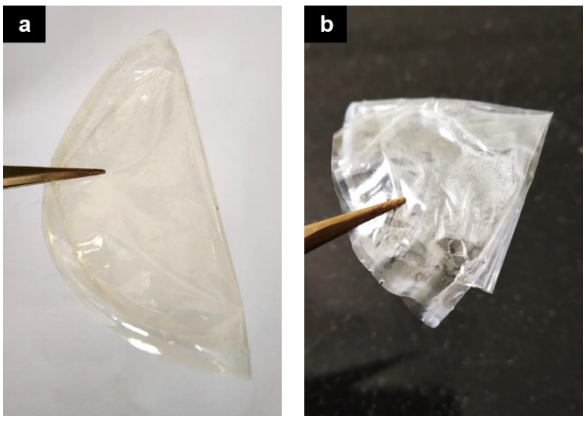

Fig. S1. Photographs of (a) **C_{60}Z-PVA** membrane and (b) PVA membrane.

Section S2. Instrumental details of physical characterisations

The, synthesized compounds were characterized and studied by various techniques to draw a comparative analysis.

Powder X-ray diffraction (PXRD) patterns were recorded on D8 Advance Bruker diffractometer using graphite monochromatic Cu Kα1 (1.5406 Å) and Kα2 (1.54439 Å) radiation. The diffraction patterns were analyzed using Bruker DIFFRAC plus EVA software.

Fourier transformed - infrared (FT-IR) spectra of the samples were recorded on an iD7 ATR Thermo Fisher Scientific-Nicolet iS5 instrument. The sample was directly put on the sample holder without any modification.

Raman spectral analysis of the samples were carried out on a WITec model Alpha 300 R Raman microscope using 785 nm laser as the excitation source. The laser intensity was maintained constant for all the samples.

N_2 gas sorption analysis of the samples were carried out on Micromeritics model ASAP 2020. All the samples were activated at 140 °C under vacuum for 12 hours, prior to N_2 sorption analysis. During the experiment, the temperature was maintained at 77 K by a liquid nitrogen bath.

Thermogravimetric analysis (TGA) of the samples were carried out on a PerkinElmer Clarus SQ 8 S mass spectrometer. All the samples were activated at 120 ℃ for 12 hours, prior to measurement.

Field emission Scanning Electron Microscope (FE-SEM) imaging was carried out on a Carl Zeiss model Ultra 55 microscope. The FESEM cross section morphology of the membrane samples were done by breaking the membranes in liquid nitrogen medium. Samples were gold coated before imaging in FESEM. **EDX** spectra and maps were recorded using Oxford Instruments X-MaxN SDD (50 mm^2) system and INCA analysis software.

Transmission electron microscope (TEM) imaging was done on a FEI (Technai Model No. 2083) instrument. The samples for TEM measurements were prepared by drop-casting a colloidal solution of the samples dispersed in methanol, on a carbon-coated copper grid and were dried in 70 °C for 24 hours.

X-ray photoelectron spectra of the samples were recorded on a Omicron, (model:1712-62-11) instrument using an Al-Kα radiation source under 15 kV voltage and 5 mA current. Prior to characterization of the samples, they were coated with a thin layer of gold to improve their electrical conductivity.

Electrochemical experiments were conducted using a Zahner Zanium electrochemical workstation operated with Thales software.

Electronic absorption spectra of the samples were recorded using a Shimadzu-2600 spectrophotometer. The solid samples were directly deposited on a barium sulphate ($BaSO_4$) bed in the sample holder and the absorption spectra were recorded in diffuse reflectance mode. The reflectance spectra were converted to absorption spectra using the Kubelka-Munk function. Quartz cuvettes of 1 cm path length were used for recording the absorbance spectrum of C_{60} in solution. The sample was prepared by ultrasonically dissolving C_{60} in n-hexane to attain a concentration of 4×10^{-5} M.

Photoluminescence (PL) measurements were carried out on a FlouroLog-3 (Horiba Jobin Yvon) spectrometer. Quartz cuvettes of 1 cm path length were used for recording the emission

profile of C_{60} in solution. The sample was prepared by ultrasonically dissolving C_{60} in toluene to attain a concentration of 1.8×10^{-3} M.

The PL of solid samples were measured by holding the sample in between two quartz plates.

Section S3. Physical characterization of C_{60}Z-n (n = A, B, C, D and E)

Section S3.1. Powder X-ray diffraction (PXRD) analysis

The PXRD patterns of all the synthesised composites in the series **C_{60}Z-n** (n = A, B, C, D and E are found to be similar to that of ZIF-8 (Fig. S2). The position of the peaks and their relative intensities matched well with the simulated PXRD pattern of ZIF-8, indicating that there has been no noticeable change in the crystal parameters of ZIF-8 due to encapsulation.

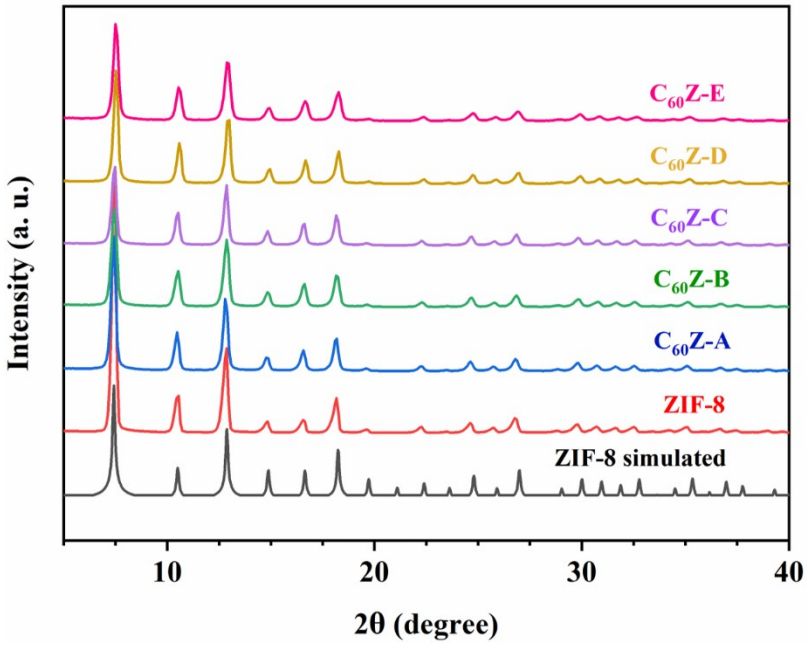

Fig. S2. PXRD patterns of simulated ZIF-8, ZIF-8 and **C_{60}Z-n** (n = A, B, C, D and E).

Section S3.2. Calculation of C_{60} loading level from CHN analysis

Table S2. CHN data of ZIF-8 and C_{60}Z.

Name of sample	C	H	N
ZIF-8	41.80	3.89	23.74
C_{60}Z-A	42.63	3.84	23.42
C_{60}Z-B	42.87	3.76	23.24
C_{60}Z-C or **C_{60}Z**	43.39	3.64	23.09
C_{60}Z-D	43.47	3.62	23.04
C_{60}Z-E	43.44	3.62	23.06

The molecular formula of ZIF-8 is $C_8H_{10}N_4Zn$.
From the CHN data of ZIF-8, the molecular formula comes out to be $C_{8.23}H_{9.20}N_{3.99}Zn$ (taking the amount of N to be standard).

Calculation of loading level of C_{60} in C_{60}Z-A:
Using similar method, from the CHN data of **C_{60}Z-A**, the molecular formula comes out to be $C_{8.49}H_{9.18}N_{3.99}Zn$ (taking the amount of N to be standard).

So, we find that there is an excess of carbon content in **C_{60}Z-A** than in ZIF-8 by ~ 0.26 per formula unit. **… (1)**

Now, each unit cell of ZIF-8 consists of 24 ($C_8H_{10}N_4Zn$) units. 4 Zn ions are situated on each face (total 6 faces) of the unit cell. Thus, each of the Zn is shared between two adjacent unit cells.
Therefore, contribution per Zn = ½.

Effective number of Zn in each unit cell = 24 × ½ =12
Thus, each unit cell has 12 ($C_8H_{10}N_4Zn$) units.
Or, each single cage of ZIF-8 consists of 12 ($C_8H_{10}N_4Zn$) units. **… (2)**

From **(1)** and **(2),** we can calculate that, for each 19 cages of ZIF-8, there is 1 C_{60} molecule in **C_{60}Z-A**.

In a similar way, the loading level of C_{60} in rest of the composites have been calculated. The respective data is presented in a tabular form below (Table S3)

Table S3. Molecular formula and loading level of C_{60} in C_{60}Z-n (n = A, B, C, D and E).

Name of sample	Molecular formula	1 C_{60} per *x* cages
ZIF-8	$C_{8.23}H_{9.20}N_{3.99}Zn$	----
C_{60}Z-A	$C_{8.49}H_{9.18}N_{3.99}Zn$	$x = 19$
C_{60}Z-B	$C_{8.60}H_{9.04}N_{3.99}Zn$	$x = 14$
C_{60}Z-C or **C_{60}Z**	$C_{8.75}H_{8.82}N_{3.99}Zn$	$x = 10$
C_{60}Z-D	$C_{8.79}H_{8.80}N_{3.99}Zn$	$x = 9$
C_{60}Z-E	$C_{8.78}H_{8.79}N_{3.99}Zn$	$x = 9$

Section S3.3. Fourier transformed - infrared (FT-IR) spectral analysis

The FT-IR spectrum of ZIF-8 shows two weak peaks at 3132 cm^{-1} and 2928 cm^{-1} for 'C–H' aromatic and aliphatic stretching, respectively (Fig. S3). A medium peak at 1586 cm^{-1} is due to 'C=N' stretching. The several peaks in the region of 1460 - 1300 cm^{-1} are a result of 2-methyl imidazole ring stretching. The two peaks at 1146 cm^{-1} and 995 cm^{-1} are due to C–N aromatic stretching and bending, respectively. The two peaks at 760 cm^{-1} and 695 cm^{-1} were owing to C–H bending and out-of-plane bending of 2-methyl imidazole ring. The strong peak at 425 cm^{-1} is because of Zn–N stretching which indicates the successful formation of the ZIF-8 framework. The FT-IR spectrum of fullerene C_{60} is rather simple with only four peaks at 527 cm^{-1}, 575 cm^{-1}, 1184 cm^{-1} and 1428 cm^{-1}, due to its highly symmetric structure. The FT-IR spectrum (Fig. S3) of **C_{60}Z** displays all the prominent features of ZIF-8 with one to one matching. Due to the very low loading of C_{60} in the composite, two of its peaks were completely masked by the features of ZIF-8 while the other two (527 cm^{-1} and 575 cm^{-1}) appear as small peaks at the same position as in free C_{60}. Two new peaks were also observed at 725 cm^{-1} and 461 cm^{-1}, apparently originating from the interaction of C_{60} and ZIF-8 framework.

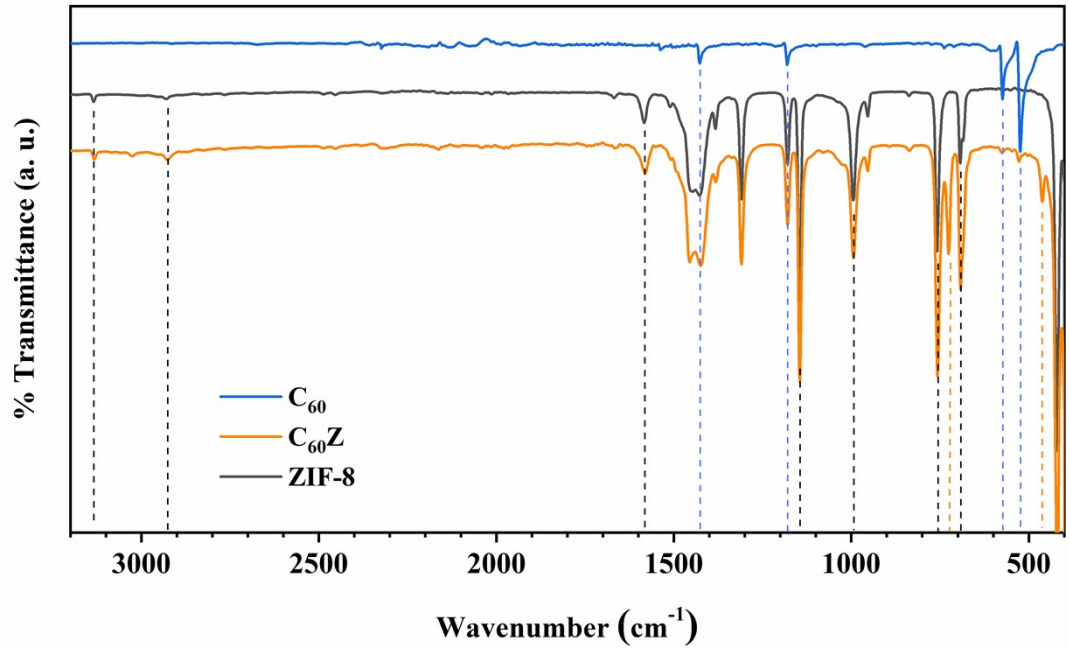

Fig. S3. FT-IR spectra of C_{60}, ZIF-8 and **C_{60}Z** (400-3000 cm^{-1}).

A comparison of the FT-IR spectra of ZIF-8 and **C_{60}Z-n (n = A, B, C, D and E)** (Fig. S4) shows that all the composites with different loading of C_{60} in them, have all the prominent features of ZIF-8. The peaks originating due to the presence of C_{60} in the composites, display a gradual increase in intensity going from **C_{60}Z-A** to **C_{60}Z-C** and then become almost constant through **C_{60}Z-D** and **C_{60}Z-E**. This is probably because the loading level of C_{60} in **C_{60}Z-C**, **C_{60}Z-D** and **C_{60}Z-E** is nearly same.

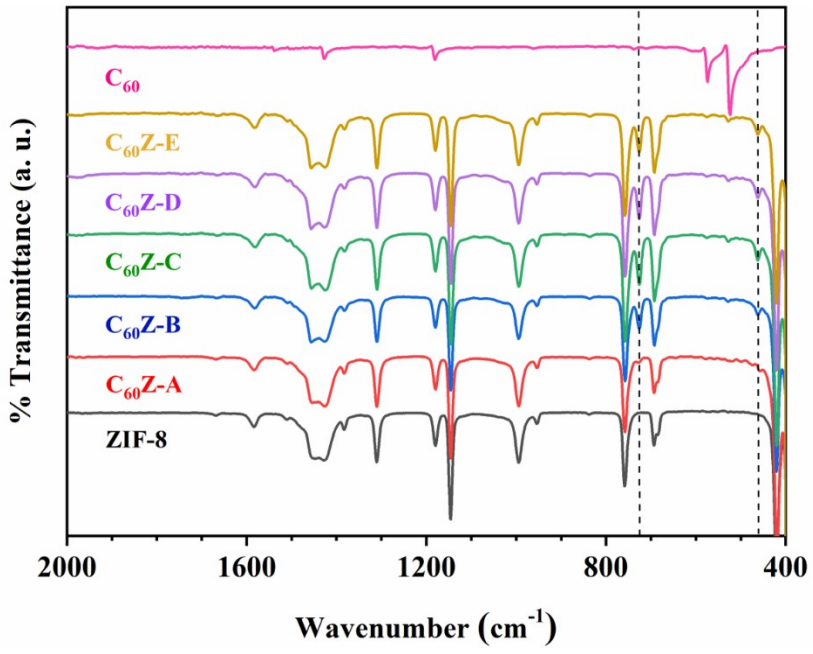

Fig. S4. FT-IR spectra of C_{60}, ZIF-8 and **C_{60}Z-n** (n = A, B, C, D and E).

Section S3.4. N_2 sorption analysis

N_2 sorption measurements were carried out for ZIF-8 and **C_{60}Z-n** (n = A, B, C and D) to understand the surface area and porosity of the samples. The sorption profiles of all the samples display Type I isotherm, which is a characteristic of microporous samples (Fig. S5). According to Brunauer–Emmett–Teller (BET) analysis, the surface area of ZIF-8, **C_{60}Z-A**, **C_{60}Z-B**, **C_{60}Z-C** and **C_{60}Z-D** are found to be 1373.72 m^2/g, 1160.09 m^2/g, 1126.34 m^2/g, 1090.83 m^2/g, and 1081.41 m^2/g, respectively. The lowering of surface area with increasing loading amount of C_{60} indicates the successful encapsulation of the C_{60} molecules.

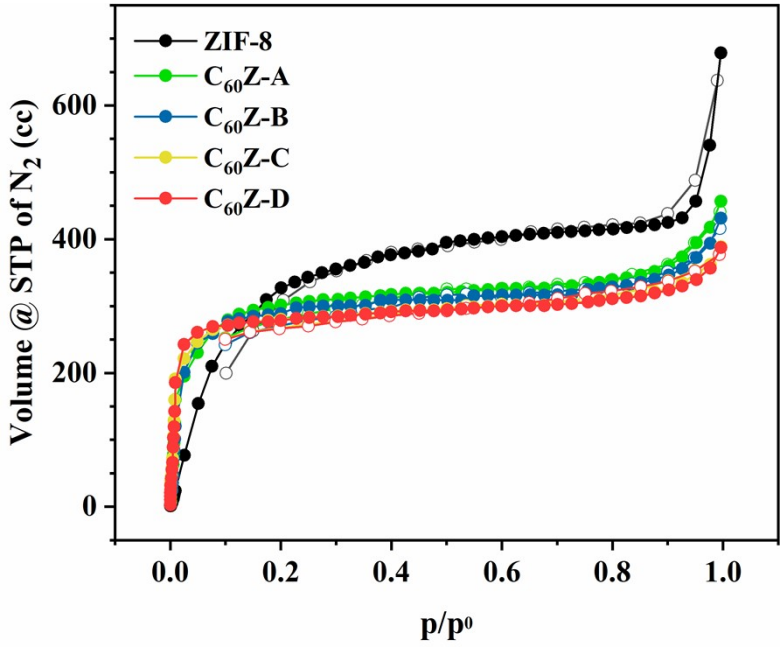

Fig. S5. N_2 gas sorption isotherms of ZIF-8 and **C_{60}Z-n** (n = A, B, C and D). Filled spheres denote adsorption and hollow spheres denote desorption experimental data points.

Section S4. Thermogravimetric analysis (TGA)

Both **C_{60}Z** and ZIF-8 started degrading from around 400 °C. By 550 °C, both of them have lost about 60% of their initial weight. The TGA curve for **C_{60}Z** has a slightly higher slope, which might be a result of interaction of C_{60} with the ZIF-8 framework. The residual mass for **C_{60}Z** found to be slightly higher than that for ZIF-8, due to the presence of C_{60}, which has a higher thermal stability (Fig. S6). The difference in residual weight (~1.24%) can be accounted for the wt% of C_{60} present in the **C_{60}Z** composite.

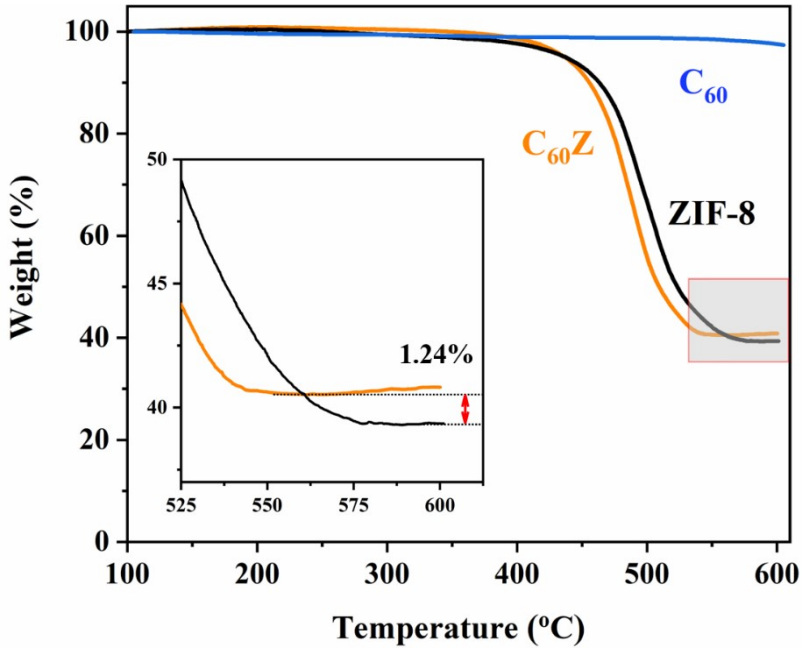

Fig. S6. TGA of C_{60}, ZIF-8 and **C_{60}Z**. Inset: magnified view of the highlighted region.

Section S5. Electronic absorption spectroscopy

The position of the peaks at 256 nm and 328 nm falling in the strong band region (200 nm – 350nm), were identical in both C_{60} (in dilute liquid solution) and **C_{60}Z** (in solid state). Since the HOMO-LUMO transitions in fullerene C_{60} is parity forbidden, the electronic spectrum displays very weak band intensity in the region of 450 nm – 650 nm. A magnified view of this region provided in the inset of Fig. S7, shows that the corresponding absorption spectra for C_{60} in solution and **C_{60}Z**, has one to one matching with one another.

In pure solid phase, C_{60} molecules stay in a closed packed structure which has a characteristic feature in its electronic spectrum.[2] On the other hand, in the case of homogeneous liquid solution state, depending on the nature of the solvent and the concentration of C_{60} in it, the molecules can stay as discrete entity or can form agglomerated phases constituting of loosely packed molecules of C_{60}. With varying extent of such assembly, the absorption spectrum of the solution changes dramatically.[3] This implies that the UV-visible spectral feature of a C_{60} molecule in true sense can only be achieved by employing a highly diluted solution of C_{60}.

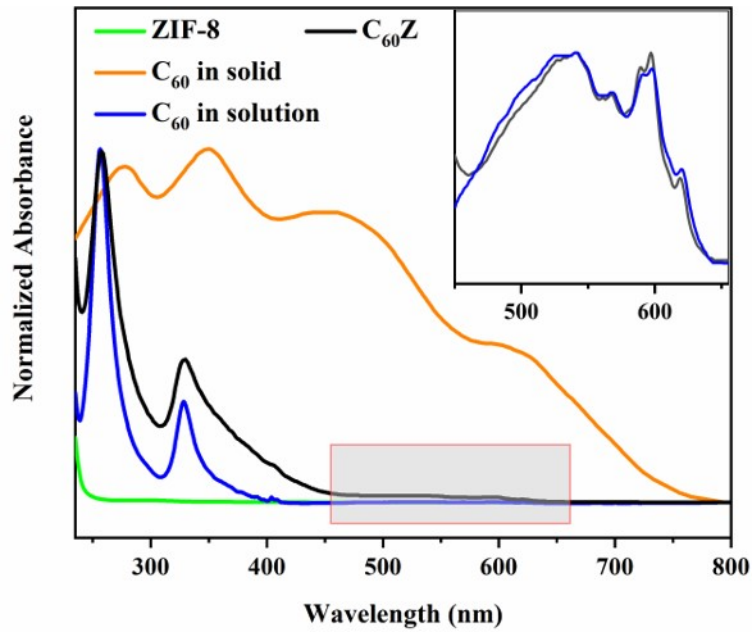

Fig. S7. Electronic absorbance spectra of C_{60} in n-hexane solution and K-M converted UV/Vis-DRS spectra of solid C_{60}, ZIF-8 and **C_{60}Z**; inset: magnified view of the highlighted region in C_{60} solution and **C_{60}Z** spectra.

Section S6. Band gap calculation of C_{60} in C_{60}Z and in dilute solution

The electronic absorption spectra were used for finding the band gap of the samples using the Tauc method. According to this method, it is assumed that absorption coefficient α can be expressed by the following equation:

$$(\alpha h\nu)^n = B(h\nu - E_g) \quad \textbf{... (1)}$$

where *h* is the Plank constant, *v* is the frequency of the radiation, B is a proportionality constant and E_g is the band gap energy.[4] For materials having allowed direct transitions, n = 2. Both fullerene C_{60} and ZIF-8 fall under this category of materials and thus for both of them n = 2. The band gap E_g for C_{60} in solution (HOMO-LUMO gap) has been calculated from its absorption spectrum using Tauc method, employing equation 1. The Tauc plot has $(\alpha h\nu)^2$ on the Y-axis and energy of the photons (*hv*) on X-axis (Fig. S10a). The point of intersection of the fitted straight line and X-axis gives the band gap energy. It was calculated to be 1.913 eV.

The band gap for **C_{60}Z** has been calculated from its absorption spectrum obtained by Kubella-Munk transformation of the diffused reflectance spectrum (DRS). The reflectance spectrum is converted to absorption spectrum using the following Kubella-Munk function:

$$F(R) = \frac{(1-R)^2}{2R} \quad \textbf{... (2)}$$

where *R* is the reflectance. Since *F(R)* is proportional to the absorption coefficient *α*, *F(R)* is substituted in place of *α* in equation 1 to give:

$$(F(R)h\nu)^n = B(h\nu - E_g) \quad \textbf{... (3)}$$

Using equation 3, the Tauc plot is generated (Fig. S10b). The band gap E_g for **C_{60}Z** is calculated to be 1.959 eV.

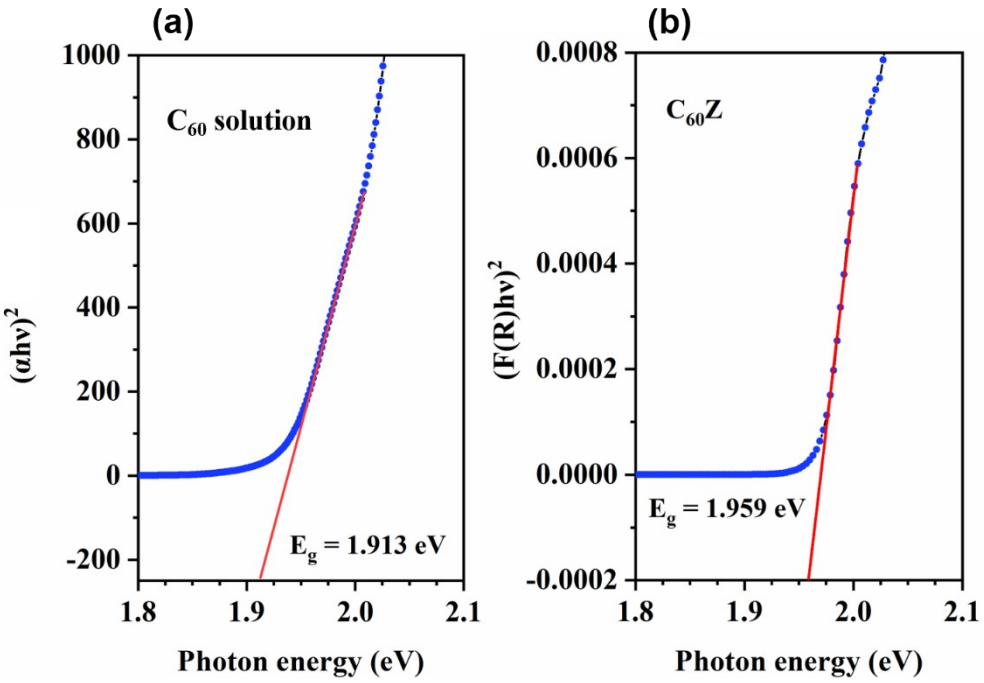

Fig. S8. Tauc plots of (a) C_{60} in solution and (b) **C_{60}Z**.

Section S7. Fluorescence emission spectroscopy

The PL spectrum of C_{60} was recorded in toluene at room temperature with excitation wavelength λ_{exc} at 450 nm. The PL spectrum of C_{60} (Fig. S9; inset) is found to be in good agreement with the previously reported data.[5] It displays a weak and broad emission feature stretching from 650 nm to 780 nm. This emission band corresponds to the $S_1(^1T_{1g}, {}^1T_{2g}, {}^1G_g) \rightarrow S_0(^1A_g)$ transition of the C_{60} molecule. But since the first excited state S_1 of the molecule is degenerate and has mixed character of $^1T_{1g}$, $^1T_{2g}$ and ^1G_g, the transition $S_0 \rightarrow S_1$ or *vice versa*, is parity forbidden. Due to this, the absorption at longer wavelength (450-650 nm) is very weak (*vide supra*) and so is the fluorescence emission (quantum yield ~ 8.5×10^{-4}). The PL emission profile of ZIF-8 was recorded in solid state with excitation wavelength λ_{exc} at 400 nm. The PL spectrum for ZIF-8 (Fig. S9) displays one strong peak centered around 445 nm, which can be attributed to the coordinated 2-methyl imidazolate of ZIF-8. The PL spectrum of **C_{60}Z** displays a strong peak around 445 nm (peak A; Fig. S9) and has a broad band of emission stretching from 540 nm to 730 nm (band B; Fig. S9). The corresponding emission profiles of ZIF-8 and **C_{60}Z** are overlaid and the intensity of both the spectra are normalised at 445 nm. The emission profiles

for the two samples match quite well for the peak at 445 nm, which means that the inherent luminescence of ZIF-8 framework of **C_{60}Z** is the sole contributor for this emission. Clearly, the emission band of **C_{60}Z** at the higher wavelength (540 nm to 730 nm) is originating from the encapsulated C_{60} molecules.

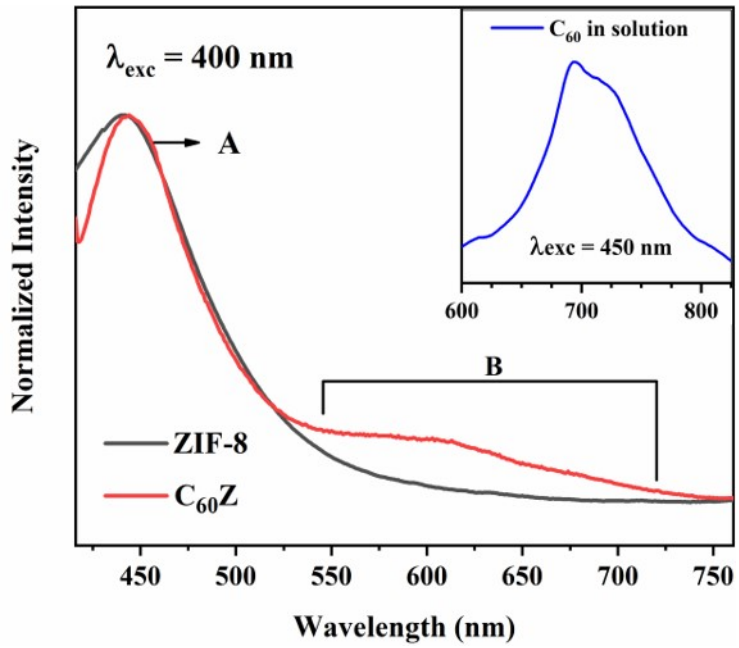

Fig. S9. Fluorescence emission spectra of ZIF-8 and **C_{60}Z** (λ_{exc} = 400 nm); inset: emission spectra of C_{60} in toluene solution (λ_{exc} = 450 nm).

Section S8. X-Ray photoelectron spectral analysis

The surface survey of both ZIF-8 and **C_{60}Z** displays signals of Au (4f and 4d), C1s, N1s, O1s, and Zn2p core levels.

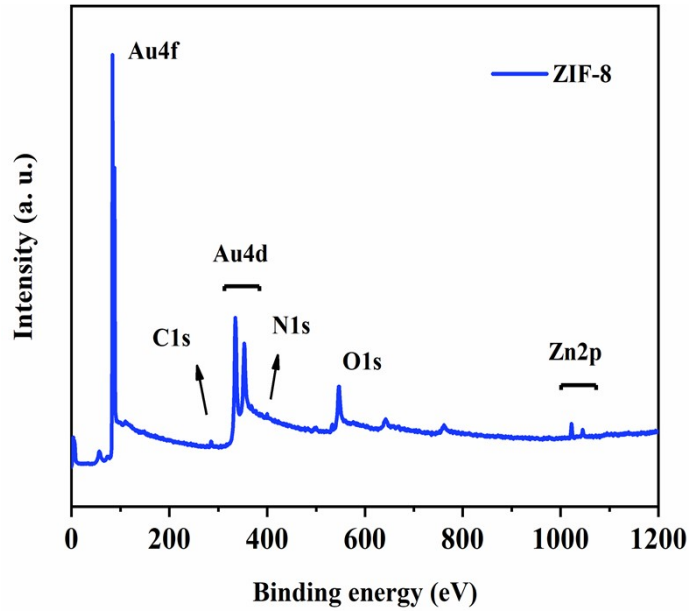

Fig. S10. XPS surface spectrum of ZIF-8.

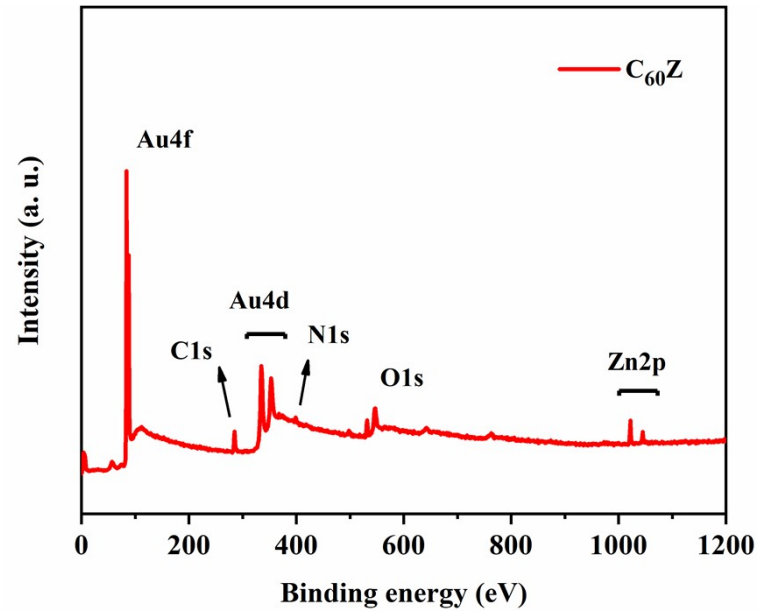

Fig. S11. XPS surface spectrum **C_{60}Z**.

Section S9. Electrochemical analysis

Section S9.1. Methodology for non-aqueous electrochemical measurements

The electrochemical measurements in non-aqueous medium were carried out in a conventional three-electrode configuration with carbon paper or modified carbon paper as working electrode and two platinum wires of suitable surface area as the counter electrode and pseudo-reference electrode, respectively. Electrochemical analysis on C_{60} was carried out in homogeneous mode employing typically 6×10^{-4} M solution of C_{60} in 0.1 M solution of tetrabutylammonium perchlorate (TBAP, supporting electrolyte) in 1:2 dry acetonitrile/toluene solvent mixture. For heterogeneous electrochemical analysis of $\mathbf{C_{60}Z}$, 4 mg of the sample was mixed with 1 mg of acetylene carbon black and 1 mL of 3:2 ethanol/water mixture. 10 µL of 5 wt% nafion (aq.) was added to it as binder. The mixture was sonicated till a homogeneous suspension was obtained. 40 µL of this homogeneous ink was then drop-casted on a carbon paper electrode and dried at 70 °C under IR lamp to obtain our $\mathbf{C_{60}Z}$ modified working electrode. 0.1 M solution of TBAP in 1:2 dry acetonitrile/toluene mixture was used as electrolyte. All the experiments were carried out under N_2 atmosphere and the electrolyte was purged with N_2 for at least 30 mins prior to each experiment. Electrochemical responses were recorded in -0.1 V/s scan rate, unless specified otherwise. All the potential values reported for non-aqueous electrochemical analysis, are with respect to ferrocene-ferrocenium (Fc^+/Fc) couple (Fig. S12).

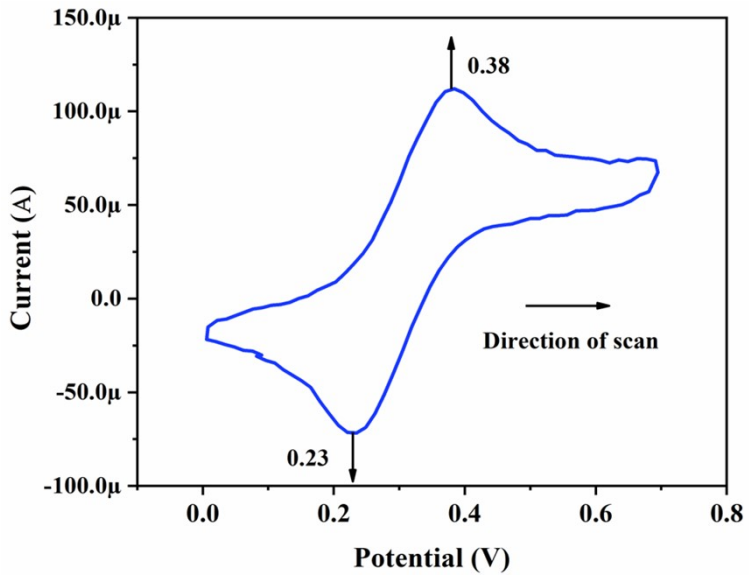

Fig. S12. Cyclic voltammogram of ferrocene showing the ferrocenium-ferrocene (Fc^+/Fc) couple. The electrochemical measurement was done in 1:2 dry acetonitrile/toluene solvent mixture taking 0.1M tetrabutylammonium perchlorate (TBAP) as the supporting electrolyte, under nitrogen atmosphere at 100 mV s^{-1} scan rate.

Section S9.2. Cyclic voltammogram and differential pulse voltammogram for $C_{60}Z$

The cyclic voltammogram of **$C_{60}Z$** (Fig. S13) recorded at 10 mV/s shows two cathodic (C1, C2) and anodic (A1, A2) responses. While A1 had a single hump centered around -0.17 V, A2 showed an overlap of two closely spaced peaks centered around -1.9 V (Fig. S13, inset), originating from C_{60}. The cathodic responses were broader than the anodic, and therefore differential-pulse voltammogram (DPV) (Fig. S13, inset) were recorded (Pulse height: 200 mV; pulse width: 0.6 s; scan rate: 50 mV s^{-1}). The DPV clearly showed two cathodic peaks centered around -0.90 V (C1) and -2.10 V (C2).

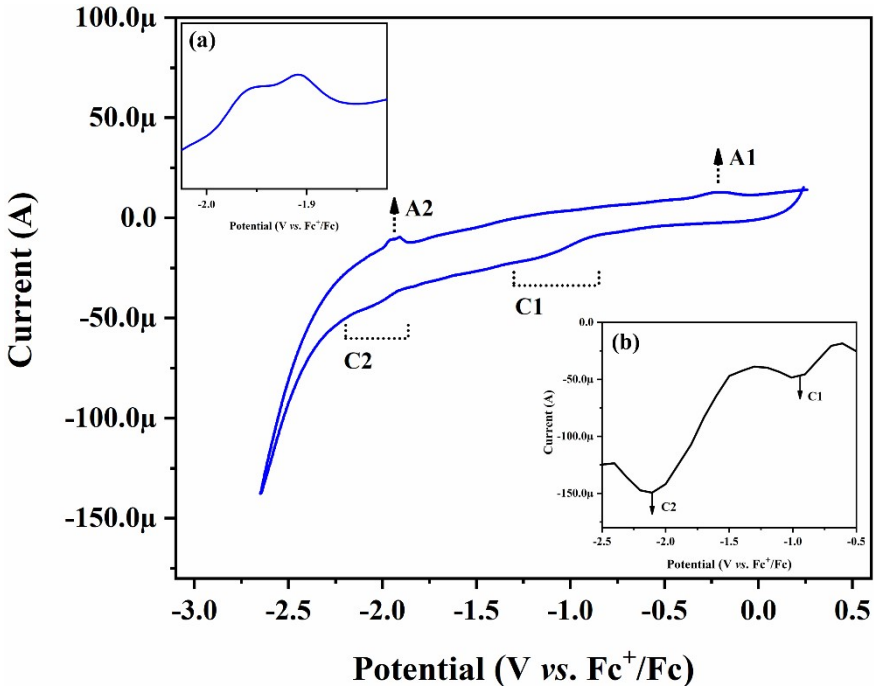

Fig. S13. Cyclic voltammogram of **$C_{60}Z$** at 10 mV s^{-1} scan rate; inset: (a) magnified view of A2 response in voltammogram; (b) differential-pulse voltammogram of **$C_{60}Z$**. The electrochemical measurement was done in 1:2 dry acetonitrile/toluene solvent mixture taking 0.1M tetrabutylammonium perchlorate (TBAP) as the supporting electrolyte, under nitrogen atmosphere.

Section S9.3. Methodology for electrocatalytic study of ORR

The electrochemical measurements for investigating oxygen reduction reaction (ORR), were carried out in a gas tight cell with three-electrode setup. Ag/AgCl was used as the reference electrode, glassy carbon as the working electrode, and Pt as the counter electrode. All the measurements for C_{60}, **$C_{60}Z$**, and ZIF-8, were done in heterogeneous mode. For all the electrochemical analysis (except for RRDE experiments), the coating sample was prepared using 4 mg of the sample, mixed with 1 mg of acetylene carbon black, 1 mL of 3:2 ethanol/water

mixture and 10 µL of 5 wt% nafion (aq.) as binder. Sample preparation for RRDE measurements required the addition of 80 µL of 5 wt% nafion (aq.) as binder. The mixture was sonicated till a homogeneous suspension was obtained. 10 µL of this homogeneous ink was then drop-casted on glassy carbon electrode/ glassy carbon ring-disk electrode and dried at 70 °C under IR lamp to obtain our catalyst modified working electrode. 0.1 M KOH was used as electrolyte. For obtaining a N_2 saturated/O_2 saturated system, the electrolyte was purged with N_2/O_2 for at least 30 mins prior to each experiment.

The electron transfer numbers (n_{RRDE}) and H_2O_2 selectivity were calculated using the following relations.[6]

$$n_{RRDE} = \frac{4N_c i_d}{N_c i_d + i_r} \quad \text{... (4)}$$

where i_d and i_r denote the disk and ring current, respectively. N_c denotes the collection efficiency of RRDE electrode which was determined to be 0.4182 (or 41.82%).

$$H_2O_2\% = 100 \times \frac{(4 - n_{RRDE})}{2} \quad \text{... (5)}$$

Section S9.4. Cyclic voltammetric and chronoamperometric analysis for $C_{60}Z$

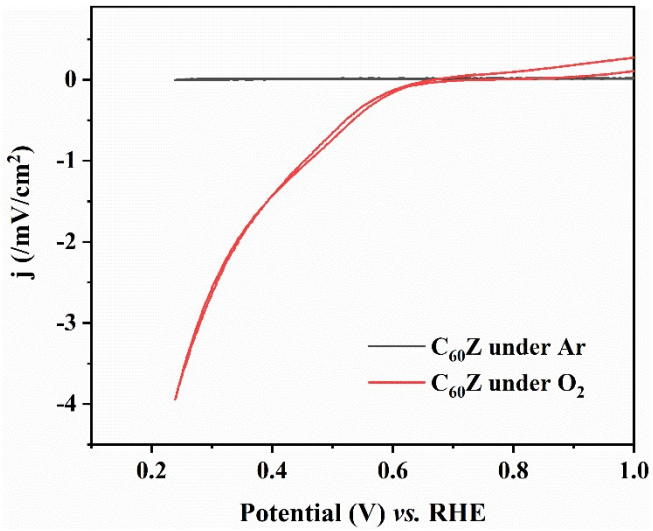

Fig. S14. Cyclic voltammograms of $C_{60}Z$ (drop cast on glassy carbon working electrode) at 100 mV s^{-1} scan rate.

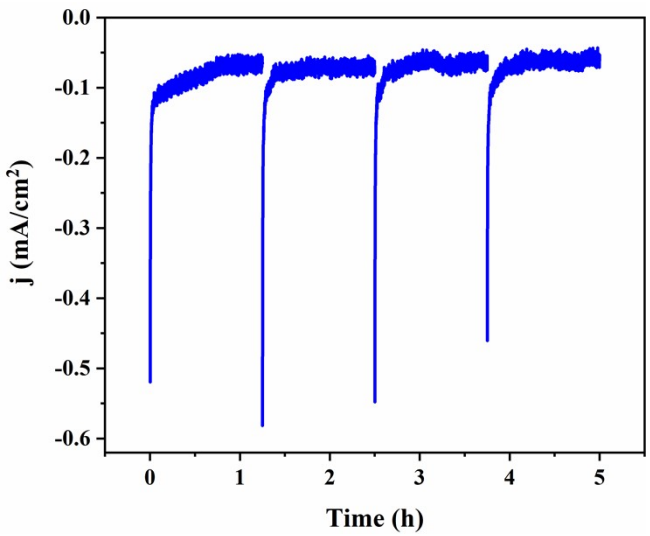

Fig. S15. Chronoamperometric analysis of **C_{60}Z** at 0.45 V (*vs.* RHE) for a total duration of 5 hours, in 0.1 M KOH. The electrolyte was purged with O_2 for 30 minutes prior to each individual measurement during the 5 h analysis.

Section S10. Controlled experiment with higher C_{60} loaded C_{60}Z composites

The synthesis of higher C_{60} loaded composites was achieved by mechanochemical technique, adapting from a recent report by V. Martinez *et al*.[7]

Synthesis of C_{60}Z – 17%: Zinc oxide (ZnO, 40 mg), 2-methyl imidazole (80 mg) and C_{60} (10 mg) were placed into a stainless-steel jar with two stainless steel balls (7 mm). The mixture was ground for 10 min at 30 Hz, followed by addition of 45 µL ethanol and 6 mg of NH_4Cl, and subsequent milling for 45 min. The product was collected by centrifugation and was washed repeatedly with ethanol and toluene (3 times each) over a course of 2 days. The product was dried at 70 °C for 24 hours.

Synthesis of C_{60}Z – 33%: The synthesis was performed using similar method as that of **C_{60}Z – 17%**. The amount of C_{60} used was 20 mg.

Both materials were structurally characterized and the loading of C_{60} in them was calculated from CHN elemental analysis.

Section S10.1. Comparison of Powder X-ray diffraction (PXRD) patterns

The PXRD patterns of the synthesised composites were found to be similar to that of ZIF-8 simulated pattern (Fig. S16). The position of the peaks matched well but their relative intensities were modified due to C_{60} encapsulation in these high loading samples.[7]

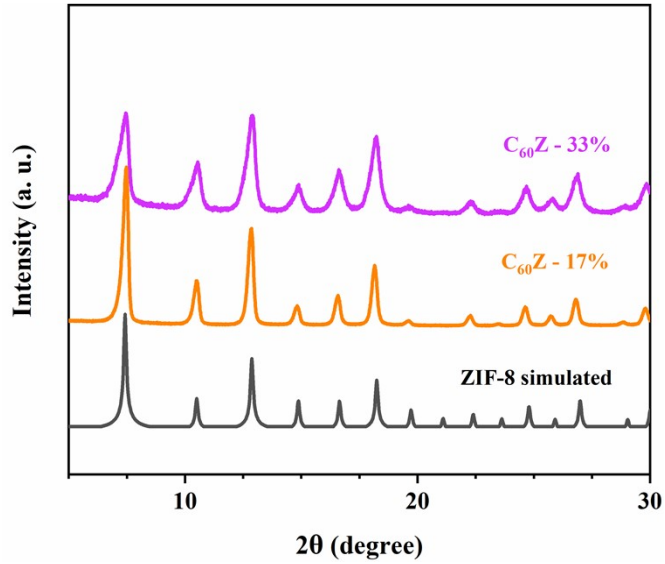

Fig. S16. PXRD patterns of ZIF-8 simulated, **C_{60}Z – 17%** and **C_{60}Z – 33%**.

Section S10.2. Comparison of Fourier transformed- infrared (FT-IR) spectra

The FT-IR spectra of the composites matched well with the reported data. The spectral feature matched predominantly with that of ZIF-8 and showed gradual increase in peak intensity originating from C_{60}.

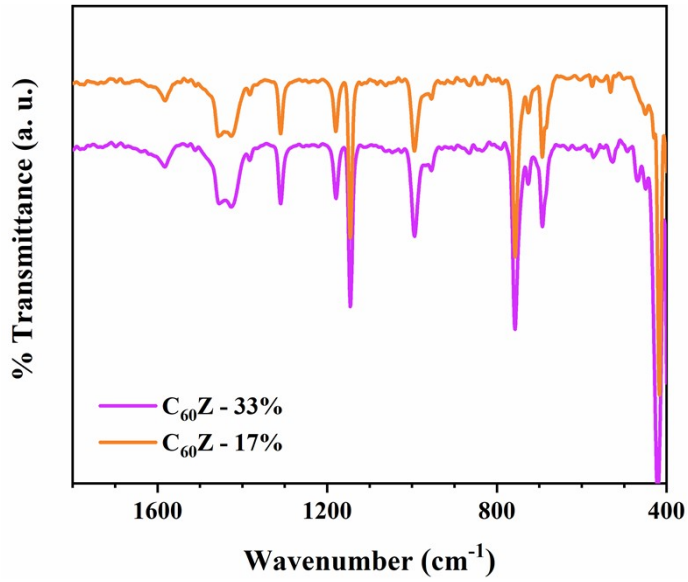

Fig. S17. FT-IR spectra of **C_{60}Z – 17%** and **C_{60}Z – 33%**.

Section S10.3. Calculation of C_{60} loading from CHN analysis

Table S4. CHN data.

Name of sample	C	H	N
C_{60}Z – 17%	44.71	4.07	23.05
C_{60}Z – 33%	46.45	3.98	21.81

The loading level of C_{60} in the composites have been calculated using same method as detailed in section S3.2. The respective data is presented in a tabular form below (Table S5).

Table S5. Molecular formula and loading level of C_{60}.

Name of sample	Molecular formula	1 C_{60} per *x* cages
C_{60}Z – 17%	$C_{9.00}H_{9.84}N_{3.99}Zn$	$x = 6$
C_{60}Z – 33%	$C_{9.91}H_{10.19}N_{3.99}Zn$	$x = 3$

Section S10.4. Comparison of Electrochemical Properties

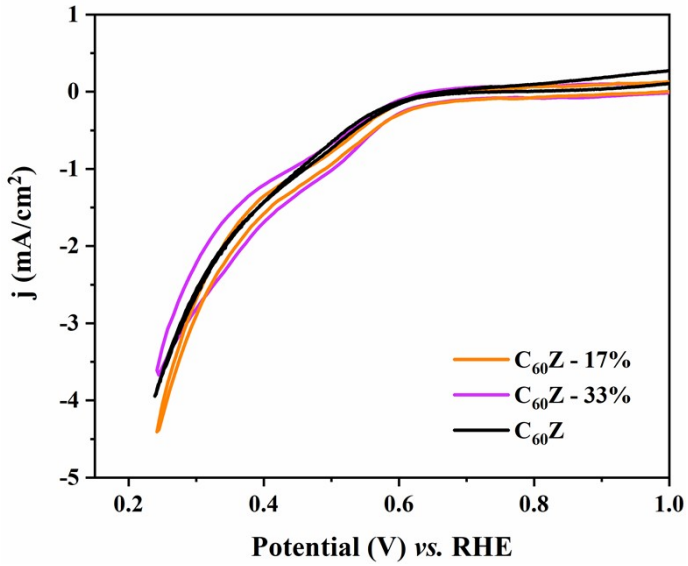

Fig. S18. Cyclic voltammograms of **$C_{60}Z$**, **$C_{60}Z$ – 17%** and **$C_{60}Z$ – 33%** at 100 mV s^{-1} scan rate. All voltammograms were recorded in O_2 saturated 0.1 M KOH.

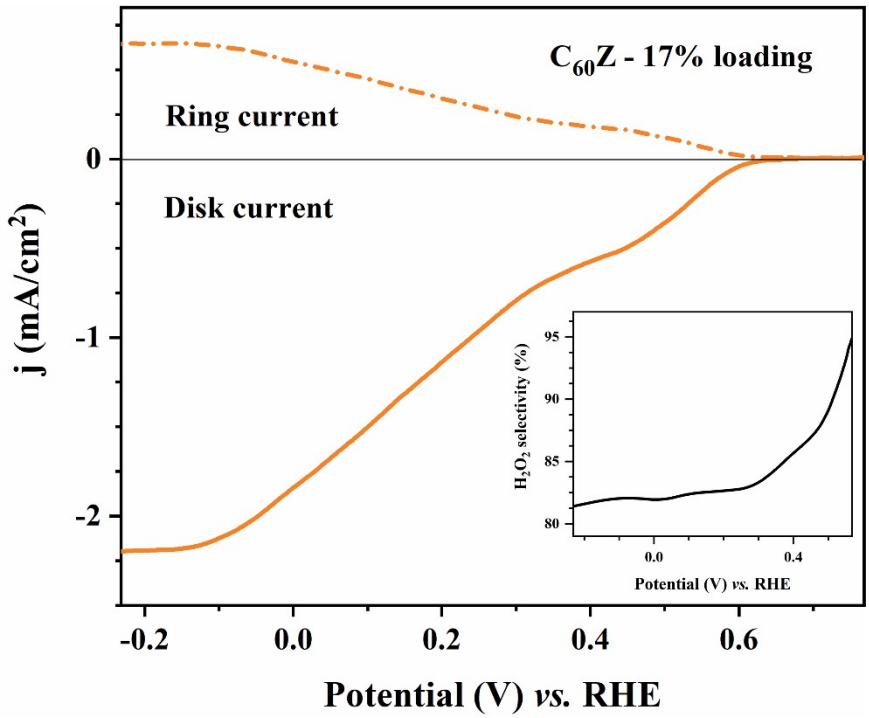

Fig. S19. Polarization curves of **$C_{60}Z$ – 17%** for oxygen reduction reaction (ORR) and H_2O_2 generation using rotating ring-disk electrode (RRDE) at 1600 rpm, and 10 mV s^{-1} scan rate. The measurements were recorded in O_2 saturated 0.1 M KOH; inset: H_2O_2 product selectivity of **$C_{60}Z$ – 17%** as obtained from the RRDE method.

Section S11. Controlled experiments to establish the encapsulation

As mentioned in the synthetic procedure, the synthesized composite **C_{60}Z** was thoroughly washed with toluene post synthesis to get rid of any adsorbed C_{60} on the MOF surface. Furthermore, to negate any possibility of any surface bound C_{60} to contribute to the observed physical and chemical properties of **C_{60}Z**, a physical mixture (C_{60}+ZIF-8) was prepared, in which the C_{60} was adsorbed onto the surface of pre-synthesized ZIF-8. The properties of (C_{60} + ZIF-8) were compared with that of **C_{60}Z** and solid C_{60} to obtain further insight about the structure-function relationship of the composite **C_{60}Z**.

(C_{60}+ZIF-8) was prepared by treating pre-synthesized ZIF-8 with a saturated solution of C_{60} in toluene for 12 hours. The product was then washed with toluene to get rid of excess C_{60} from the MOF surface. This way it was ensured that the C_{60} present is only surface adsorbed. The synthetic procedure also ensures that none of the C_{60} molecules get encapsulated in the ZIF-8 pores, but only get adsorbed on the surface.

Section S11.1. Comparison of Powder X-ray diffraction (PXRD) patterns

The PXRD pattern of (C_{60}+ZIF-8) displayed features corresponding to both C_{60} and ZIF-8 (Fig. S20), as opposed to **C_{60}Z**, whose PXRD pattern matched completely with that of pure ZIF-8.

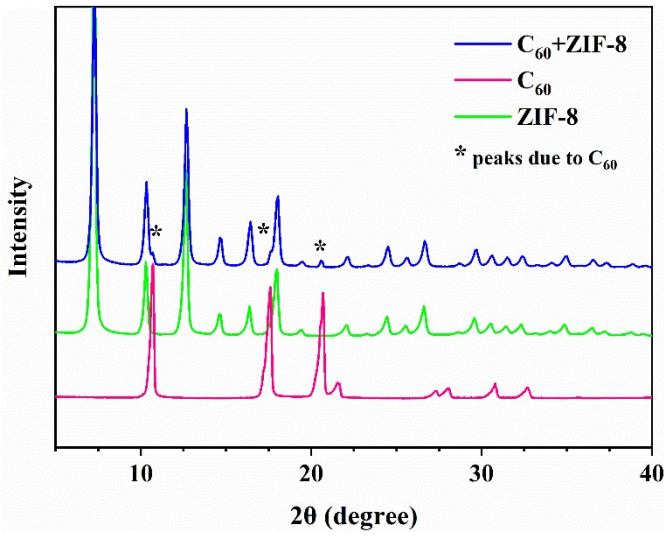

Fig. S20. PXRD patterns of ZIF-8, C_{60} and (C_{60}+ZIF-8).

Section S11.2. Comparison of Fourier transformed- infrared (FT-IR) spectra

The FT-IR spectra of (C_{60}+ZIF-8) (Fig. S21) shows all the prominent features of ZIF-8. Due to the low quantity of fullerene C_{60} in (C_{60}+ZIF-8), the peaks at 1184 cm^{-1} and 1428 cm^{-1} corresponding to C_{60}, were masked by the features of ZIF-8. Although the strong peaks at 527 cm^{-1} and 575 cm^{-1} appeared at the same position as non-encapsulated C_{60}. But the new peaks at 725 cm^{-1} and 461 cm^{-1}, originating from the host-guest interaction in **C_{60}Z**, were not found in (C_{60}+ZIF-8). This suggests that the fullerene adsorbed on the ZIF-8 surface of (C_{60}+ZIF-8) do not possess similar strong interaction with the MOF framework, which is present for the encapsulated fullerenes in **C_{60}Z**.

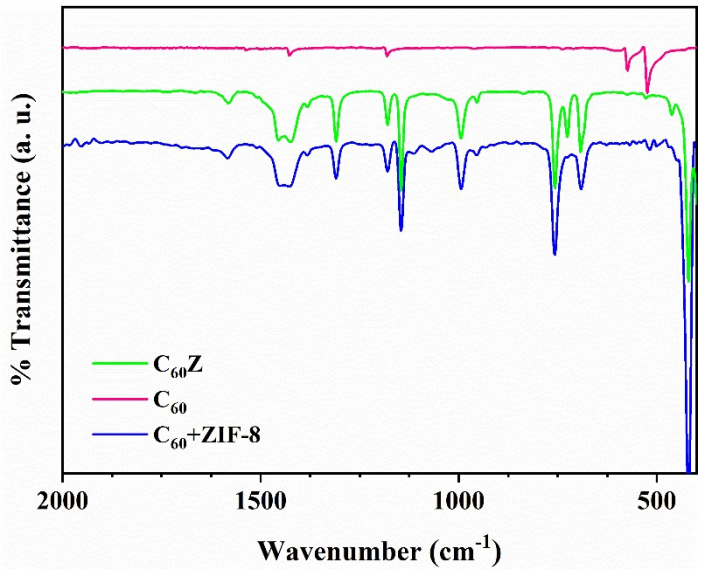

Fig. S21. FT-IR spectra of solid C_{60}, **C_{60}Z**, and (C_{60}+ZIF-8).

Section S11.3. Electronic absorption spectroscopy

The UV-Visible (recorded in diffused reflectance mode) spectrum of the (C_{60}+ZIF-8) was comparable to that of C_{60} solid (non-encapsulated) and was widely different from **C_{60}Z** composite (Fig. S22). The broad peaks in the 400 nm -700 nm region suggests that the (C_{60}+ZIF-8) cannot provide a molecular level spatial separation for the C_{60} on the surface of ZIF-8. The surface bound C_{60} in this case can interact with each other and behave similar to solid aggregates

of C_{60} to some extent. It is well-known that with variation in particle size of fullerene aggregates, the electronic spectrum changes dramatically.[2]

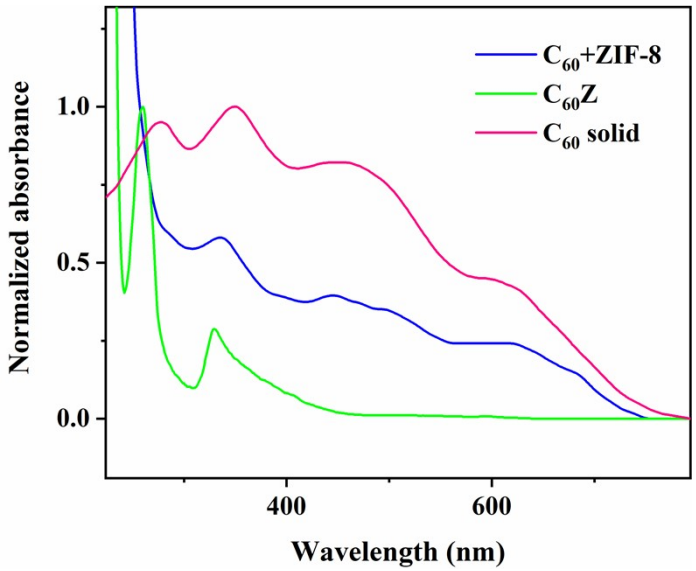

Fig. S22. K-M converted UV/Vis-DRS spectra of solid C_{60}, **C_{60}Z**, and (C_{60}+ZIF-8).

Section S11.4. Calculation of C_{60} content in (C_{60}+ZIF-8) from CHN analysis

Table S6. CHN data.

Name of sample	C	H	N
C_{60} + ZIF-8	43.84	4.11	23.19

The content of C_{60} in the physical mixture has been estimated using similar method as detailed in section S3.2. The composition of the mixture is $C_{8.80}H_{9.90}N_{4.00}$. This gives an excess of ~0.57 carbon due to C_{60} per formula unit of ZIF-8, which gives almost same amount of C_{60} content in the physical mixture as compared to **C_{60}Z**.

The above-mentioned XRD, UV-Vis (DRS) and FT-IR spectral analysis along with electrochemical ORR performance of (C_{60}+ZIF-8) physical mixture when compared with that of C_{60} and **C_{60}Z**, it infers the following important information: (1) The (C_{60}+ZIF-8) samples has presence of crystalline planes corresponding to solid C_{60} (Fig. S20), which further indicates a lack of molecular level spatial separation in the (C_{60}+ZIF-8) physical mixture where the C_{60}

species are only adsorbed by the MOF surface; (2) The FT-IR spectrum of (C_{60}+ZIF-8) (Fig. S21) is basically the summation of FT-IR spectra of C_{60} and ZIF-8 in accordance with their relative abundance in the (C_{60}+ZIF-8) physical mixture; (3) UV-Vis (DRS) spectrum of (C_{60}+ZIF-8) (Fig. S22) is similar to C_{60} solid and varies widely from **C_{60}Z** indicating a further similarity of (C_{60}+ZIF-8) to the electronic structure of solid C_{60}; a noteworthy point to establish lack of molecular level interaction between the MOF and the surface bound C_{60} species unlike the encapsulated C_{60} species in case of **C_{60}Z**. Thus, it could be inferred that, **C_{60}Z** is not a mere case of surface adsorbed C_{60} onto ZIF-8 surface but a molecular level confinement into the cavity of ZIF-8 to form a host-guest composite material where the ZIF-8 acts as the host and the C_{60} acts as the guest. This inference was further strongly supported by the electrochemical ORR performance of the (C_{60}+ZIF-8) physical mixture (Fig. 5a, 5b, 5c, in the main manuscript). The ORR properties of the (C_{60}+ZIF-8) physical mixture was similar to that of solid C_{60} to some extent and varied widely from that of **C_{60}Z**. With the help of these controlled experiments, it was confirmed that **C_{60}Z** composite was not a case of MOF surface bound C_{60} molecules but is a host-guest composite material.

Section S12. Physical characterization of C_{60}Z-PVA membrane

Section S12.1. Powder X-ray diffraction (PXRD) analysis

The diffraction pattern of **C_{60}Z-PVA** membrane (Fig. S23) displays all the features of pure PVA membrane along with some of the prominent peaks of **C_{60}Z**. There were no noticeable changes with respect to broadening or shifting of peaks compared to pure PVA membrane, indicating similar crystallinity even after incorporation of **C_{60}Z** nanofillers.

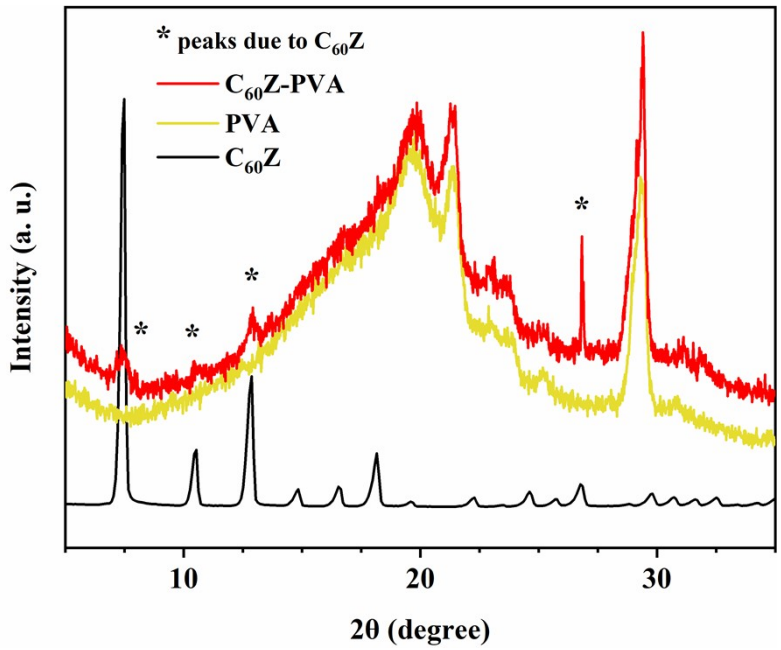

Fig. S23. PXRD patterns of **C_{60}Z**, **C_{60}Z-PVA** and PVA.

Section S12.2. Fourier transformed - infrared (FT-IR) spectral analysis

The FT-IR spectrum of **C_{60}Z-PVA** (Fig. S24) membrane predominantly consists of the spectral features of PVA polymer. However, several small peaks (marked with *) could be found originating from the **C_{60}Z** nanocomposite. There were no noticeable changes in the position of the peaks, indicating that the molecular structure of **C_{60}Z** was unaltered even after the process of membrane fabrication.

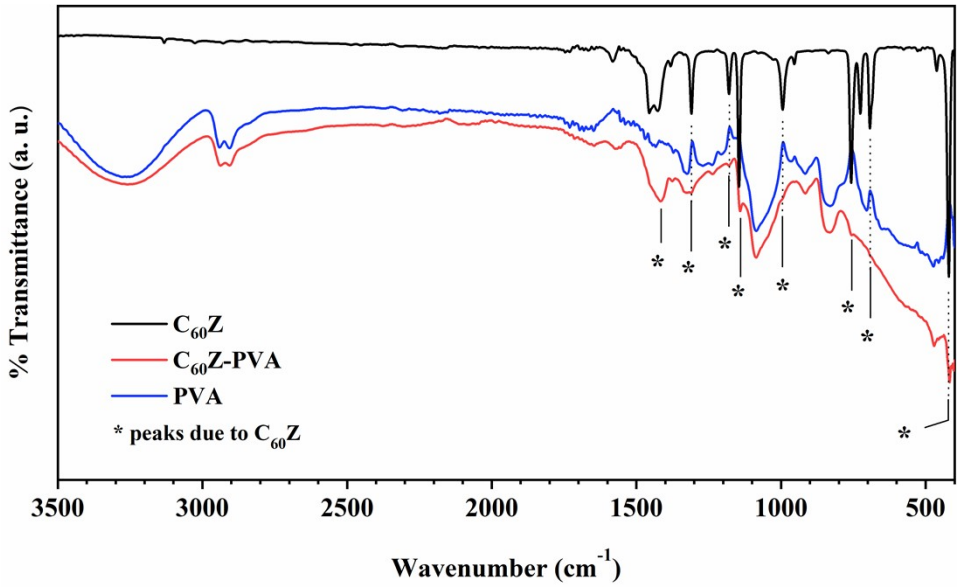

Fig. S24. FT-IR spectra of **C_{60}Z**, PVA and **C_{60}Z-PVA**.

Section S12.3. FESEM images

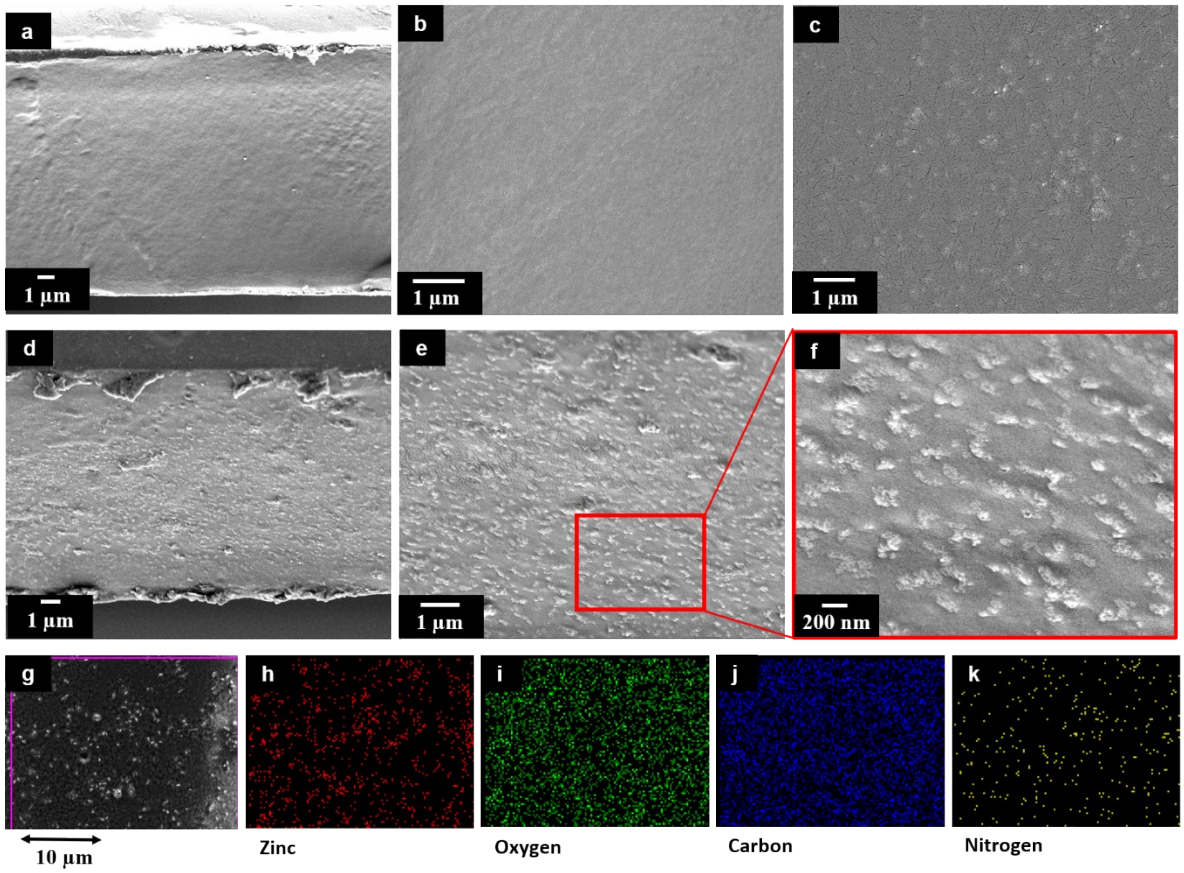

Fig. S25. FESEM images of (a) PVA membrane cross-section; (b) surface of PVA membrane; (c) surface of **C_{60}Z-PVA** membrane; (d) cross-section of **C_{60}Z-PVA** membrane; (e) dispersed **C_{60}Z** nanofillers in the cross-section of **C_{60}Z-PVA** membrane; (f) magnified view of the nanofillers. (g-k) EDX mapping of **C_{60}Z-PVA** membrane showing uniform dispersion of **C_{60}Z**.

Reference

[1] S. Mukhopadhyay, A. Das, T. Jana and S. K. Das, Fabricating a MOF Material with Polybenzimidazole into an Efficient Proton Exchange Membrane, *ACS Appl. Energy Mater.,* 2020, **3**, 7964- 7977.

[2] J. Lee, M. Cho, J. D. Fortner, J. B. Hughes and J – H. Kim, Transformation of Aggregated C_{60} in the Aqueous Phase by UV Irradiation, *Environ. Sci. Technol.,* 2009, **43**, 4878–4883.

[3] N. O. Mchedlov-Petrossyana, N. N. Kamneva, Y. T. M. Al-Shuuchi, A. I. Marynin and S. V. Shekhovtsov, The peculiar behavior of fullerene C_{60} in mixtures of 'good' and polar solvents: Colloidal particles in the toluene–methanol mixtures and some other systems, *Colloids and Surfaces A: Physicochem. Eng. Aspects,* 2016, **509**, 631–637.

[4] P. Makuła, M. Pacia and W. Macyk, How To Correctly Determine the Band Gap Energy of Modified Semiconductor Photocatalysts Based on UV–Vis Spectra, *J. Phys. Chem. Lett.,* 2018, **9**, 6814-6817.

[5] V. S. Pavlovich and E. M. Shpilevsky, Absorption and fluorescence spectra of C_{60} fullerene concentrated solutions in hexane and polystyrene at 77–300 K, *J. Appl. Spectrosc.,* 2010, **77**, 335-342.

[6] A. Hasanzadeh, A. Khataee, M. Zarei and Y. Zhang, Two-electron oxygen reduction on fullerene C_{60}-carbon nanotubes covalent hybrid as a metal-free electrocatalyst, *Scientific Reports,* 2019, **9***,* 13780.

[7] V. Martinez, B. Karadeniz, N. Biliškov, I. Lončarić, S. Muratović, D. Žilić, S. M. Avdoshenko, M. Roslova, A. A. Popov and K. Užarević, Tunable Fulleretic Sodalite MOFs: Highly Efficient and Controllable Entrapment of C60 Fullerene via Mechanochemistry, Chem. Mater., 2020, **32**, 10628−10640.